Afinogenov, Boris I.; Kopylova, Daria S.; Abrashitova, Ksenia A.; Bessonov, Vladimir O.; Anisimov, Anton S.; Dyakov, Sergey A.; Gippius, Nikolay A.; Gladush, Yuri G.; Fedyanin, Andrey A.; Nasibulin, Albert G.

Midinfrared Surface Plasmons in Carbon Nanotube Plasmonic Metasurface

Published in:
Physical Review Applied

DOI:
10.1103/PhysRevApplied.9.024027

Published: 26/02/2018

Document Version
Publisher's PDF, also known as Version of record

Please cite the original version:
Afinogenov, B. I., Kopylova, D. S., Abrashitova, K. A., Bessonov, V. O., Anisimov, A. S., Dyakov, S. A., Gippius, N. A., Gladush, Y. G., Fedyanin, A. A., & Nasibulin, A. G. (2018). Midinfrared Surface Plasmons in Carbon Nanotube Plasmonic Metasurface. *Physical Review Applied*, *9*(2), 1-9. Article 024027.
https://doi.org/10.1103/PhysRevApplied.9.024027

Midinfrared Surface Plasmons in Carbon Nanotube Plasmonic Metasurface

Boris I. Afinogenov,[1,*] Daria S. Kopylova,[1] Ksenia A. Abrashitova,[2] Vladimir O. Bessonov,[2] Anton S. Anisimov,[3] Sergey A. Dyakov,[1] Nikolay A. Gippius,[1] Yuri G. Gladush,[1] Andrey A. Fedyanin,[2] and Albert G. Nasibulin[1,4,†]

[1] *Skolkovo Institute of Science and Technology, Moscow 143026, Russia*
[2] *Faculty of Physics, Lomonosov Moscow State University, Moscow 119991, Russia*
[3] *Canatu Oy, Konalankuja 5, FI-00390 Helsinki, Finland*
[4] *Department of Applied Physics, Aalto University, P.O. Box 15100, FI-00076 Espoo, Finland*

(Received 26 October 2017; revised manuscript received 21 November 2017; published 26 February 2018)

We report an experimental observation of the midinfrared surface plasmon excited in a carbon nanotube plasmonic metasurface. The absorption of a 400-nm-thick single-walled carbon nanotube film perforated with laser-drilled subwavelength holes arranged in a 2D lattice is resonantly enhanced by 75% as compared with the unstructured film. The enhancement of absorption has a resonant behavior associated with the excitation of the surface plasmon and occurs at the wavelengths around 15 μm for the lattice period of 10 μm. The spectral position and the magnitude of the resonance are controlled entirely by the structure geometry and can be tuned in a broad range. We demonstrate that periodic patterning can be applied to tailor the bolometric performance of carbon nanotube thin films. Namely, the voltage response of the metasurface is enhanced by 100% at the wavelength of the plasmon resonance as compared with the unstructured film. We discuss mechanisms of the enhancement and compare experimental results with the finite-difference time-domain and scattering-matrix method simulations.

DOI: 10.1103/PhysRevApplied.9.024027

I. INTRODUCTION

Surface plasmons (SPs) which are localized modes of the electromagnetic field excited at an interface of positive- and negative-index media are now being utilized in different areas of science and technology. Plasmonic structures are used in sensing [1,2], nonlinear optics [3,4], and nanophotonics [5]. Since SP modes are characterized by the large enhancement of the electromagnetic field, plasmonic metasurfaces are being investigated to improve light harvesting efficiency in solar cells [6–8] and to overcome low intrinsic absorption of monolayer graphene [9–13]. In plasmonic structures, the field is primarily localized in the dielectric adjacent to metal, which results in an additional absorption in the vicinity of SP resonance [14,15]. Since metals have extremely large dielectric constants in the visible and IR ranges, the field does not penetrate deeply into the volume of the metal itself, and excitation of SPs on metals patterned with subwavelength holes does not affect absorption much, but rather leads to an extraordinary optical transmission [16,17]. However, it was shown that absorption of semicontinuous metal films could be tailored upon SP excitation [18].

Single-walled carbon nanotubes (SWCNT) have high electrical conductivity [19] and great thermal conductance [20] combined with excellent chemical stability. Other important features of SWCNTs are mechanical strength and high elasticity [21,22]. Those properties determined SWCNTs utilization for applications in rigid [23–25] and flexible transparent electronics [26–29] as well as in optoelectronics [30–32]. Transparency, great electrical properties, and inherent nanometer size of SWCNT have motivated the interest to the SWCNT plasmonics. Despite the fact that localized plasmons in individual CNTs were successfully predicted and observed recently [33–36], very few papers report on the study of propagating SPs excited in the bulk CNT film. It was shown that SWCNT films could be used to create plasmonic and metamaterial devices with tunable response operating in the terahertz spectral range [37,38].

One of the many applications of SWCNT is a detection of infrared light in a bolometric scheme. Pure SWCNT have a temperature coefficient of resistance (TCR) on the order of 1% K^{-1} and relatively high absorption in the near-IR region which yields a good voltage response even to a weak light. Starting from the pioneering work of Itkis *et al.* [39] many studies were performed to increase the efficiency of SWCNT-based bolometers. Embedding SWCNTs to the polymer [40–42] leads to the growth of the composite TCR up to 10% K^{-1} which is greater than the TCR of commercially used vanadium oxide [43] and silicon and also improves the mechanical stability of the device. The drawback of the composite bolometers is the longer

*boris.afinogenov@skolkovotech.ru
†a.nasibulin@skoltech.ru

response time determined by a larger amount of material which has to be heated. Another approach to improve the performance of bolometers is to increase the absorption of the electromagnetic radiation in an active area of a bolometer. This was realized in near-IR and terahertz ranges using plasmonic nanoantennas to localize the incident field in the SWCNT network [44,45].

In this paper, we experimentally demonstrate the excitation of a mid-IR surface plasmon in a periodically structured single-walled carbon nanotube film. We show that patterning of a SWCNT film with micrometer-sized holes leads to an absorption enhancement by 75% in the vicinity of surface-plasmon resonance wavelength. The room-temperature bolometric response is shown to be enhanced in the same range by 100% in comparison with an as-prepared film. We use scattering-matrix method (SMM) and finite-difference time-domain (FDTD) simulations to explain the observed phenomena.

II. METHODS AND SAMPLES

SWCNTs are synthesized with an aerosol CVD (catalyst floating) technique [46], which provides films of cottonlike randomly oriented nanotubes. Films used in the experiment had thicknesses of 150 nm and are mechanically merged into the stack of three. The resultant films are suspended over a 6-mm opening between two gold electrodes. A schematic drawing of the sample is shown in Fig. 1(a).

To perform microstructuring, we mount the sample on the motorized stage allowing for the translation of the entire sample with 100-nm accuracy in the range of 0–30 mm. Holes in the film are drilled with a femtosecond laser focused onto the sample with a 20× objective. Upon irradiation with the femtosecond laser pulses, CNTs in the focal volume decompose to carbon monoxide and carbon dioxide while adjacent regions are not heated. A detailed description of the fabrication setup along with the video of the fabrication process can be found in Appendix A. A scanning electron micrograph of the structured film is shown in Fig. 1(b). Holes are arranged in the 2D square lattice with a period of 10 μm, thus forming a plasmonic metasurface. In the paper we discuss two samples of metasurfaces with hole diameters of 3 and 2 μm. In the visible light, the structure appears in rainbow colors due to diffraction, and two parts of the sample can be easily distinguished by the naked eye [see inset of Fig. 1(b)].

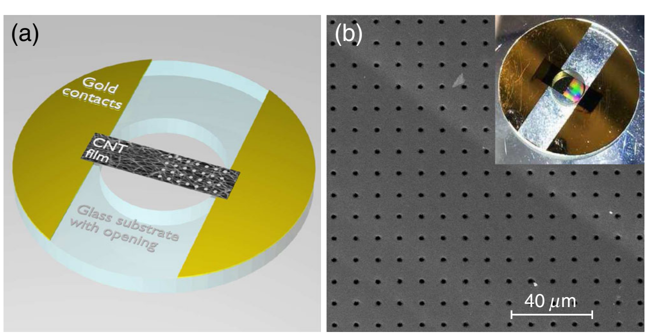

FIG. 1. (a) Illustration of the sample. (b) Scanning electron micrograph of the structured part of the SWCNT film. The inset shows a photograph of the ribbon sample. The right part appears in rainbow colors due to the film structuring.

The total area of the metasurface is 3×3 mm^2, and the same area is left unstructured for the proper reference measurements. For the measurements in the bolometer regime, the film is cut with a laser to form a ribbon to avoid parallel shunting. Thus, the resultant sample is a series of unstructured and metasurface areas between electrodes as shown in Fig. 1(a).

Transmittance and reflectance spectra are measured with a *Brucker Vertex 70v* FTIR spectrometer at the angle of incidence of 10° with the resolution of 4 cm^{-1}. To measure the spectral characteristics of the bolometer voltage sensitivity, we use the sample as a detector of the spectrometer. The diameter of the IR beam is 0.5 mm. All studies are performed at room temperature and the ambient pressure of 1 mbar.

III. RESULTS AND DISCUSSION

Solid curves in Fig. 2(a) show transmittance and reflectance spectra of the unstructured SWCNT film. Both transmittance and reflectance have resonances around the wavelength of 2.5 μm attributed to the E_{11} electronic transition in individual SWCNTs composing the film. With the increase of the wavelength, transmittance starts to grow, and reflectance tends to decline until approximately 5 μm. For the wavelengths larger than 5 μm optical properties of the SWCNT film are similar to those of a typical metal below its plasma frequency [47]. In the range of 5–50 μm the transmittance monotonically declines while the reflectance monotonically grows.

Transmittance and reflectance of the SWCNT metasurface shown by the dashed curves in Fig. 2(a) behave differently. The transmittance of the metasurface is higher than the transmittance of the unstructured film, which is attributed to the lesser amount of material. The reflectance of the metasurface is lower in the entire spectral range. At the wavelengths around 15 μm resonance features are observed in both transmittance and reflectance spectra. Resonances are associated with a SP excitation and have a typical Fano shape: dip-peak and peak-dip for transmittance and reflectance, respectively.

Absorption of both parts of the sample is calculated as $A = 1 - R - T$. The relative absorption enhancement is obtained as $\Delta A = [(A_{\mathrm{MS}} - A_{\mathrm{film}})/A_{\mathrm{film}}]$, where A_{MS} and A_{film} are absorptions of the metasurface and unstructured areas of the sample, respectively. Spectral dependence of the ΔA is shown in Fig. 2(b) with black dots. As it is discussed, absorption of the metasurface is lower for the short wavelengths because of the lesser amount of

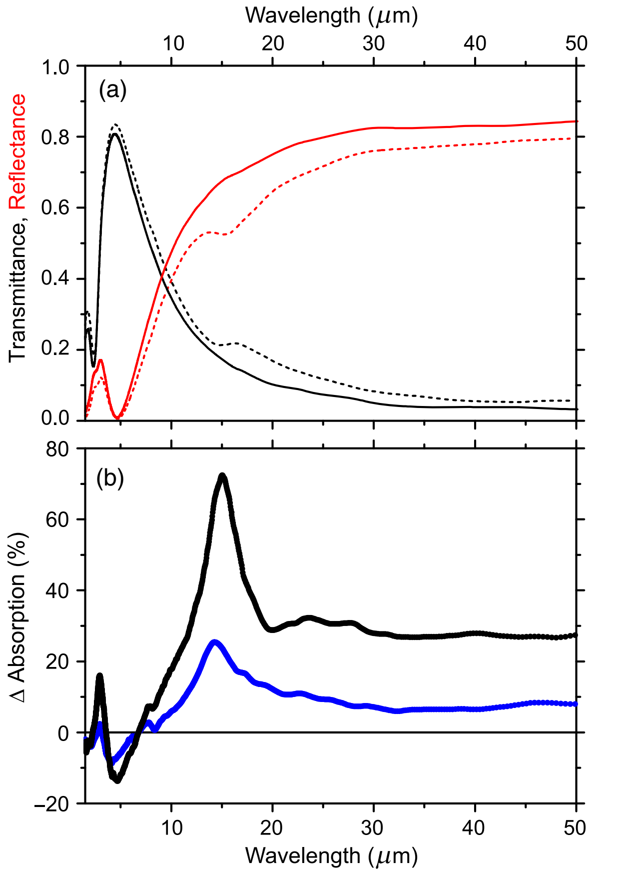

FIG. 2. (a) Reflectance and transmittance spectra of the unstructured (solid curves) and metasurface (dashed curves) areas of the sample. (b) Spectral dependence of the absorption enhancement in the metasurface in comparison with the unstructured SWCNT film. The hole size is 3 μm (black dots) and 2 μm (blue dots).

SWCNT. Starting from 5 μm, it grows, and a sharp peak is observed in the vicinity of the SP resonance. For the wavelengths in the range, 25–50 μm the absorption enhancement remains above zero with an average level of 30%. Blue dots in Fig. 2(b) show the spectral dependence of the ΔA in the metasurface comprising 2-μm holes. The SP in this sample is excited at the same wavelength of 15 μm, however, the corresponding absorption enhancement is lower. The ΔA in the SP resonance maximum is 25% and the long-wave background is 10%.

To demonstrate the idea of carbon-nanotube SP application, we use the SWCNT metasurface as a bolometer and measured the spectrum of its voltage sensitivity. Bolometer voltage sensitivity R_V is related to the absorption as

$$R^V = \frac{IR\alpha AR_{\rm th}}{\sqrt{1+\omega^2\tau^2}}, \quad (1)$$

where I is a current through the bolometer, R is a sample resistance, $\alpha = 1\%$ is TCR, $R_{\rm th}$ is a thermal resistance, ω is a light modulation frequency, and τ is a bolometer response time [48]. Thus, a bolometer with the enhanced absorption should have the greater sensitivity if bias current and resistance remain constant. To fulfill the last condition, the unstructured and the metasurface areas of the sample are connected in a series and only one of them is illuminated at the time while the other is screened. Data on the absolute spectral sensitivity of the continuous SWCNT film in the mid-IR range of spectrum can be found in Ref. [49] and are omitted in this article. Relative enhancement of the bolometer response $\Delta R^V = (R^V_{\rm MS} - R^V_{\rm film})/R^V_{\rm film}$ versus the wavelength of the IR radiation is shown in Fig. 3. The behavior of the response enhancement closely resembles that of the absorption enhancement. At short wavelengths, the bolometer response of the SWCNT metasurface is slightly weaker than the response of the continuous SWCNT film except for the range of the E_{11} transition wavelength. With the increase of the wavelength, the enhancement starts to grow until approximately 15 μm, where it peaks at 100%. For the wavelengths exceeding 22 μm the enhancement remains at the level of 20%. The spectral dependence of the ΔR^V in the metasurface comprising 2-μm-sized holes is shown in Fig. 3 with blue dots. Enhancement of the voltage response in the metasurface with smaller holes is lower in the entire spectral range. The maximum measured ΔR^V at the SP resonance wavelength is 40%.

It should be noted that values of absorption enhancement and bolometer response enhancement are different with the last being larger in the spectral range 2–20 μm. Since resistance, TCR, current, and light modulation frequency remain the same for both parts, the difference between ΔA and ΔR^V is the most likely attributed to the change in

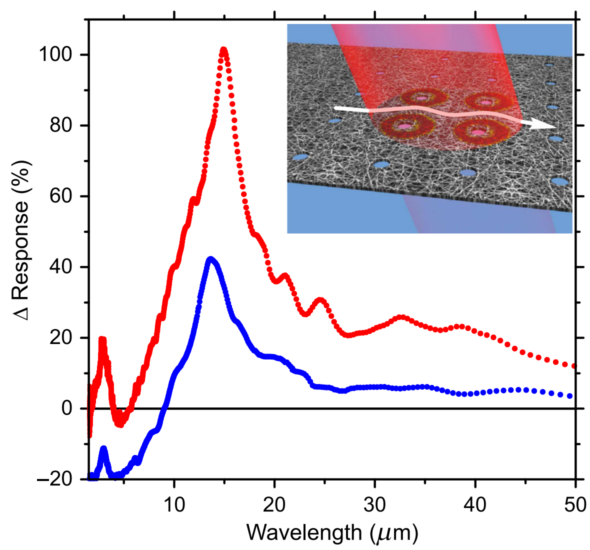

FIG. 3. The spectrum of the voltage response enhancement in the structured SWCNT film compared to the unstructured film. The inset shows a schematic of the current flow in the film under IR irradiation.

thermal resistance. Indeed, thermal resistance is defined as $R_{\mathrm{th}} = L/SG$, where L is the length of the sample, G is the SWCNT film specific thermal conductivity, and S is the cross-sectional area. Upon drilling the holes in the SWCNT film, an effective cross section is reduced which increases R_{th}. In the range of longer wavelengths, however, the response amplification is weaker than the absorption enhancement. To explain this phenomenon, we first describe the theoretical model and results of numerical calculations.

As it is noted, in the wavelength range greater than 5 μm the spectral dependences of transmittance and reflectance of the unstructured SWCNT film remind one of those of metal. For the sake of modeling, we can describe the SWCNT film in an effective medium approximation (EMA) with the Drude dispersion law $\varepsilon(\omega) = \varepsilon_\infty - [\omega_p^2/(\omega^2 + i\omega\gamma)]$. Parameters of the model are estimated as $\varepsilon_\infty = 2.843$, $\hbar\omega_p = 383$ meV, and $\hbar\gamma = 14.07$ meV. Calculated spectra of transmittance and reflectance of the model medium along with the experimental spectra of continuous SWCNT film are shown in Fig. 4(a). It can be seen that experimental and numerical transmittance spectra match well assuming experimental errors. Measured transmittance is slightly lower for the wavelengths between 5–7 μm, which is the most likely attributed to the inaccuracy of the dispersion modeling in the epsilon-near-zero region.

Periodic structuring of a uniform film with a Drude dispersion should lead to the excitation of propagating SPs at wavelengths close to the period of the structure. Those surface waves manifest themselves as Fano-type resonances in spectra of transmittance and reflectance. For the studied metasurface, the resonances appear at the wavelengths between 12 and 17 μm, as shown in Fig. 4(b). It is seen that the SP resonances in experimental and numerical spectra have the same spectral position, but the calculated resonances are slightly sharper. This discrepancy originates from the nonuniformity of the film thickness, deviations in the hole diameter, and nonzero angular divergence of the IR beam.

Figure 4(c) shows FDTD-calculated distributions of the electric field in a unit cell of the metasurface with the EMA dispersion at the SP resonant wavelength of 15 μm for the TM-polarized radiation. Calculations bolster the plasmonic nature of the resonance as characteristic in-plane, and perpendicular field distributions are observed. SPs, in this case, are propagating along the x axis and cause additional absorption in the SWCNT film. In addition to the propagating SP, a localized plasmon (LP) is excited in the structure. It appears as the hot spot at the edge of the hole in the SWCNT film. The electric field of the LP mode is primarily localized outside the film. However, inside the SWCNT film, the field is also enhanced in a direct vicinity of the hole edge. This gives an additional contribution to the absorption of IR radiation.

At the long wavelengths away from the SP resonance, absorption of the metasurface is larger than the absorption of the unstructured area by 30%. This phenomenon is not related to the excitation of the surface electromagnetic wave and will appear in any perforated material even if holes compose the aperiodic structure. To qualitatively explain the observed behavior we assume that the transmittance at long wavelengths is equal to zero. The reflectance for the normally incident radiation is given by the Fresnel equation,

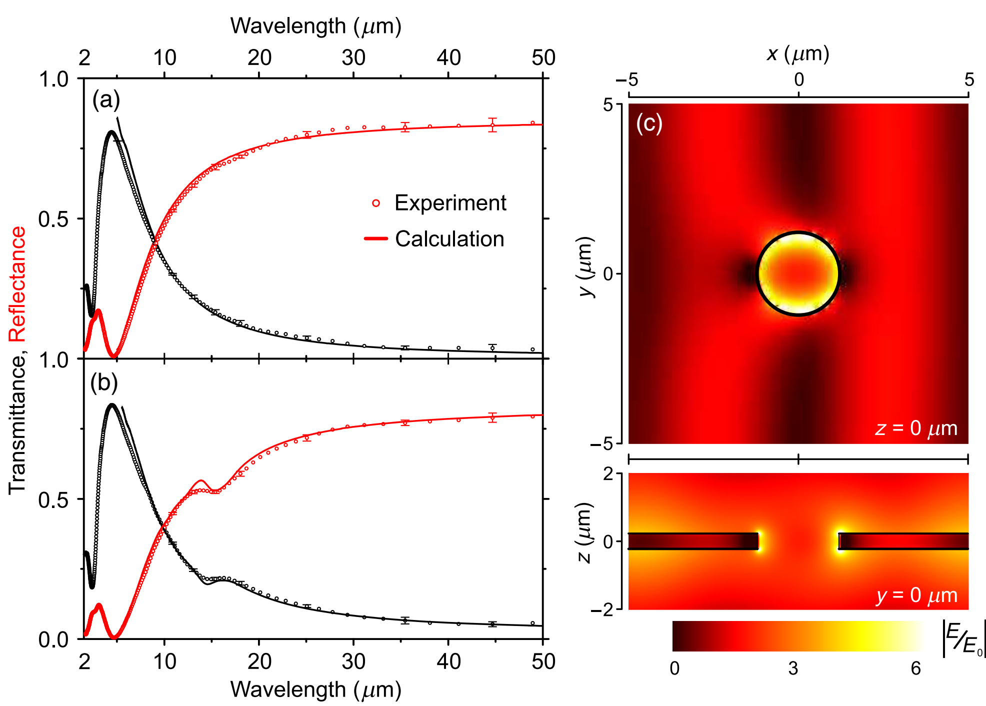

FIG. 4. Experimental (open dots) and numerical (solid curves) spectra of transmittance and reflectance of an (a) unstructured SWCNT film and (b) perforated SWCNT film. (c) FDTD-calculated distributions of the electric field in the structured film at the wavelength of 15 μm.

$$R = \left|\frac{\tilde{n}-1}{\tilde{n}+1}\right|^2, \quad (2)$$

where $\tilde{n}$ is a complex index of refraction. The absorption in this assumption is calculated as $A = 1 - R$. At the wavelength of 30 μm $\tilde{n}$ of SWCNT film is $1.50 + 8.74i$ and the calculated absorption is 0.0726. Drilling 3-μm holes arranged in a square lattice with a period of 10 μm can be interpreted as replacing 7% of SWCNT volume with air. According to Maxwell Garnett equation $\tilde{n}$ of the perforated film becomes $1.42 + 8.28i$. The calculated absorption of the perforated film equals 0.0765, which is only 5% larger as compared to the unstructured SWCNT film although in the experiment and numerical calculations the long-wave absorption is shown to be enhanced much larger. The additional absorption in a perforated film arises from the field localization in hot spots along the edge of the hole. Away from the SP resonance, the electric field hot spots appear alone, and their characteristic size and field magnitude decrease with the increase of the wavelength. Continuous film at the long wavelengths effectively screens electromagnetic radiation, so the amount of material interacting with light and absorbing it is low. A hole in the film and the hot spot near its edges causes more material to interact with the external field. Additional absorption is determined by the area of interaction which grows with the increase of a hole diameter and thickness of the film.

Dependence of the electric field hot spot's size on the wavelength is also responsible for the discrepancy in absolute values between absorption gain and voltage response gain. As we discussed earlier, response enhancement is larger than the absorption enhancement at the short wavelengths, while with the increase of wavelength it becomes significantly less. For the short wavelengths, the absorption takes place in the whole volume of the metasurface unit cell [see Fig. 4(c)], thus, the additional heat is distributed across the metasurface almost uniformly. For the longer wavelengths, only a small amount of the metasurface volume close to the edges of the holes is being heated and experiences a change in resistance. Since SWCNTs have a positive TCR, the current in the SWCNT film tends to bypass areas with the increased resistance as illustrated in the inset of Fig. 3. Such localized heating results in a drop in the voltage response as compared with the overall sample absorption concerning a heat transfer.

To investigate the scope of tuning the SP resonance wavelength and the corresponding absorption peak magnitude, we perform numerical calculations using the scattering-matrix method [50]. This technique is much faster for the simulation of the optical response as compared with the FDTD method. For the SMM calculations we use the described Drude dispersion of the SWCNT material; the number of harmonics is 625. Figures 5(a)–5(c) show the absorption of the SWCNT metasurface with 3-μm-sized holes arranged in a square lattice with a period of 10 μm versus the wavelength normalized to the period and the in-plane wave vector for TE-, TM-, and unpolarized light, respectively. The bright stripe in Fig. 5(a) corresponds to the localized surface plasmon (LP) mode. The field distribution of this mode is shown in Fig. 4(c). The dependence for the TM-polarized light shows a low dispersion LP curve which is hybridized with the propagating SP modes. As we work for a small angle of incidence of 10°, only such hybrid mode is observed experimentally in unpolarized light. For the normal incidence, the resonant frequency of the SP is 0.7 (15 μm), and it slowly shifts to the higher frequencies with the increase of the wave vector. It should also be noted that the Q factor of the SP mode reduces with the increase of the wave vector as the resonant frequency approaches the plasma frequency of the SWCNT film. For the experimental conditions, the SP Q factor is equal to 92 with the corresponding propagation length of 200 μm.

Figure 5(d) shows the dependence of the absorption enhancement in the metasurface on the wavelength and the period of the structure. The hole diameter is assumed to be 3 μm. Since the SP is excited using a grating coupling method, the metasurface period significantly affects the SP resonant wavelength. In the structure with a 15-μm period, the SP is excited at the wavelength of 20 μm. With the decrease of the period, the SP resonant wavelength blueshifts: it is 10 μm for the structure with the period of 5 μm. The magnitude of the corresponding absorption peak increases with the decrease of the period. This increase is most likely attributed to the decrease of the SP Q factor as a real part of the SWCNT dielectric function diminishes.

Dependence of the SP resonant wavelength on the thickness of metal was predicted theoretically in 1957 [51] and recently has been demonstrated experimentally [52]. It is shown that for very thin films the SP frequency is significantly redshifted as compared with the SP excited in semi-infinite metal. With the increase of the film thickness, the resonant frequency rapidly blueshifts and saturates. For noble metals, the "saturation" thicknesses are in the order of several tens of nanometers. For the SWCNT film, however, this phenomenon can be observed for relatively large thicknesses, as shown in Fig. 5(e). The SP resonant wavelength rapidly redshifts starting from the film thickness of 400 nm. With the decrease of the film thickness, the absorption enhancement also drops.

The resonant wavelength and magnitude of the SP-associated peak in absorption also depend on the hole size. For the metasurface with the fixed period of 10 μm this dependence is shown in Fig. 5(f). For the hole sizes in the range between 0.2–0.6 of the structure period, the resonant wavelength has no spectral shift. However, the magnitude of the corresponding absorption peak grows by the reasons discussed earlier. With the further increase of the hole size, the SP-resonant wavelength slightly shifts to the blue part of the spectrum. Additionally, a second resonance arises

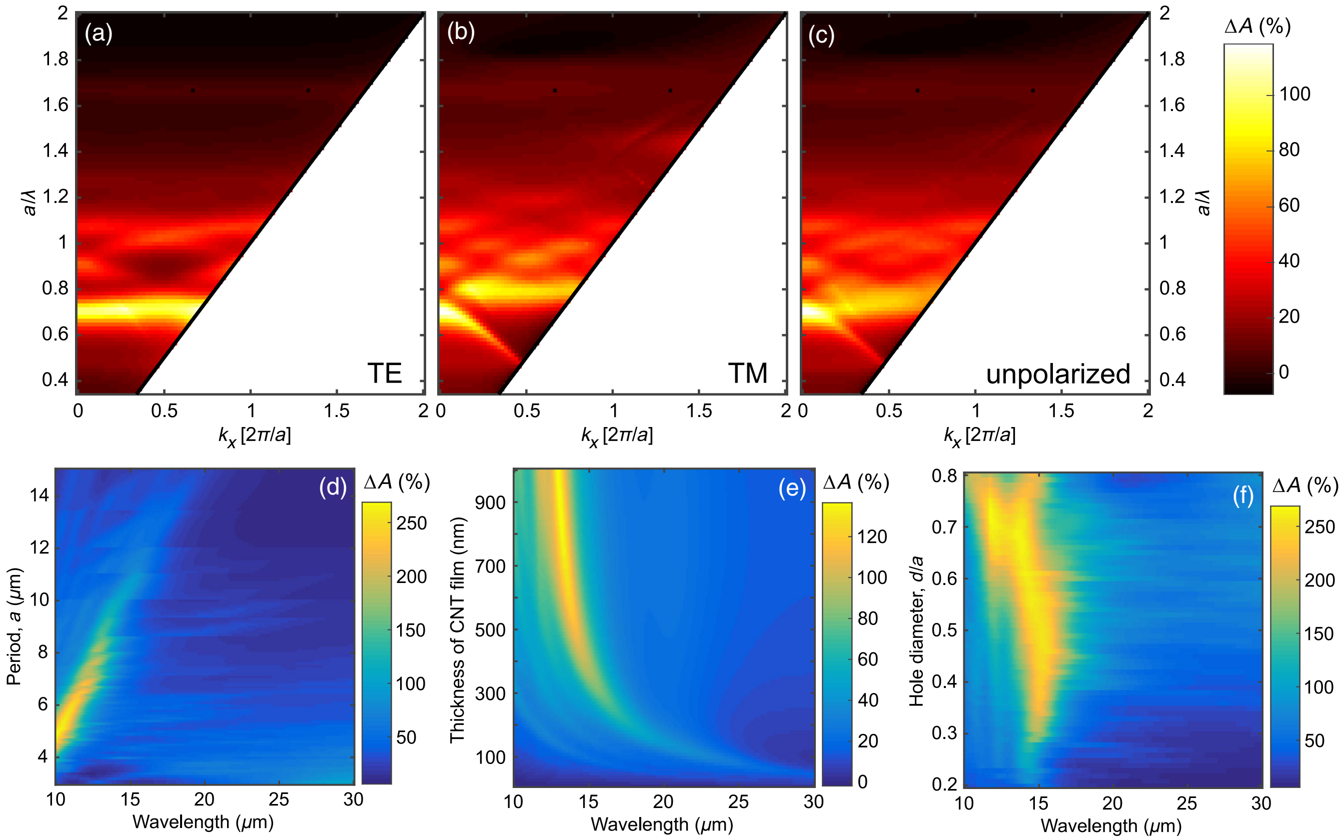

FIG. 5. (a)–(c) Absorption of the SWCNT metasurface versus normalized wavelength and in-plane wave vector for different polarizations of the IR light. (d) Absorption enhancement versus wavelength and period of the metasurface. The hole diameter is 3 μm; the film thickness is 400 nm. (e) Absorption enhancement versus wavelength and size of the holes normalized to the period. The metasurface period is 10 μm; the film thickness is 400 nm. (f) Absorption enhancement versus wavelength and SWCNT film thickness. The hole diameter is 3 μm; the period of the metasurface is 10 μm.

in the spectrum at the shorter wavelengths. Absorption enhancement peaks at 250% for the structure comprising holes for which the diameter is 0.7 of the structure period.

IV. CONCLUSIONS

We demonstrate that a carbon nanotube metasurface supports the excitation of the midinfrared surface plasmon. The SP excitation significantly enhances absorption and room-temperature bolometric response of the film. For the studied sample, patterned with 3-μm holes arranged in a 2D square lattice with a 10-μm period, absorption enhances by 75% as compared with the unstructured SWCNT film. The voltage response of the SWCNT bolometer is enhanced by 100% at the wavelength of 15 μm. Our numerical studies have shown that the observed phenomena can be quantitatively described using an effective medium approximation for a SWCNT film.

Our method applies to improve the performance of all current SWCNT bolometers and is fairly scalable for mass manufacturing.

ACKNOWLEDGMENTS

The Russian Science Foundation is greatly acknowledged for financial support (Agreement No. 17-19-01787).

APPENDIX A: MICROFABRICATION SETUP

For the fabrication of SWCNT metasurfaces, we use a custom-built setup, originally constructed for two-photon absorption lithography [53]. The scheme of the setup is shown in Fig. 6. As a source of radiation the femtosecond Ti:sapphire laser (*Coherent Vitara*) is used. It delivers 60-fs-long pulses with a central wavelength of 800 nm. The average power at the output of the laser is 500 mW. An acousto-optic modulator (AOM) is used as the fast shutter with a rise and fall time of fewer than 0.5 μs. The power of the radiation is controlled by the system of the half-wave plate ($L/2$) mounted in the motorized stage and the Glan-Taylor prism (GP). The photodiode (PD) is used to monitor power after the control system. The accuracy of power control is 0.5 mW in the range of 5–100 mW.

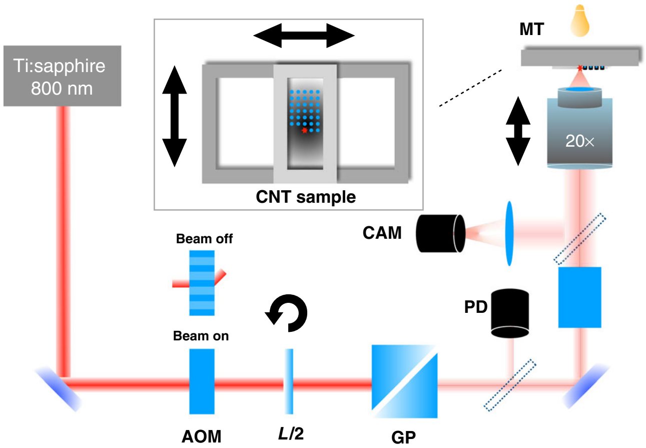

FIG. 6. Scheme of the microfabrication setup.

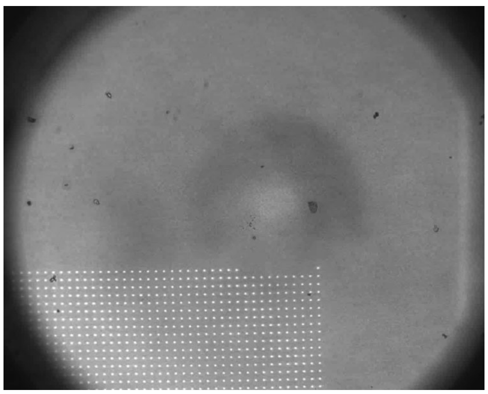

VIDEO 1. The process of drilling holes in a SWCNT film.

Samples of SWCNT films are mounted onto the motorized microscope table (MT) (Thorlabs). It had a travel range of $11.5 \times 7.5\ \mathrm{cm}^2$ with a 100-nm precision. To focus femtosecond radiation onto the sample, we use the air objective (LOMO, 20×, NA = 0.4) mounted in the piezoelectric stage (Newport). The latter is used to provide coincidence of the sample and objective focal plane. The stage could move by a maximum of 200 μm with an accuracy of 5 nm.

The structuring process is visualized and controlled *in situ* by a CCD camera (CAM) (Thorlabs). It is crucial for manufacturing to find the optimal parameters such as power and exposition time. They should guarantee that SWCNTs are completely removed in the focal volume while the rest of the film is not heated much. The best results are achieved with 45 mW of incident power at 200-ms exposition time. The total time required to drill one hole is about 1 s, including time for the MT positioning and autofocusing. The drilling process recorded by CCD is shown in Video 1. To characterize holes, we use scanning electron microscopy. According to SEM images, holes have straight edges and are almost free of SWCNTs. The mean measured diameter is 3 μm.

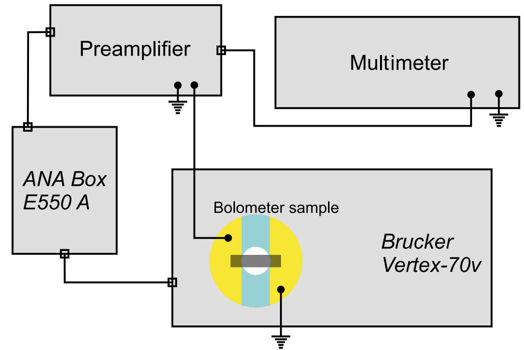

FIG. 7. Scheme used to measure bolometer spectral characteristics.

APPENDIX B: BOLOMETER VOLTAGE SENSITIVITY MEASUREMENTS

To measure the bolometer's spectral characteristics a standard Globar, embedded in *Vertex 70v* FTIR spectrometer, is used as a source of radiation [49]. The spectrum of the Globar is close to the blackbody spectrum. The modulated radiation of the Globar is fed to the sample which is placed in the sample chamber of the spectrometer. Thin wires are soldered to the gold contact pads of the sample and to the input of a special low-noise two-cascade preamplifier. Its first-cascade gain could be varied depending on the load resistance: $K_{\mathrm{amp}} = R_{\mathrm{fb}}/R_{\mathrm{bol}}$, where R_{fb} is the feedback resistance, which equals either 10 or 100 kΩ depending on the switch position; R_{bol} is the resistance of the bolometric sample. A preamplifier is connected to the spectrometer input through the *Brucker ANA Box E550A* console, which serves as an analog-to-digital converter and an additional preamplifier. The voltage of ± 12 V is fed to the preamplifier from a low-noise source of the spectrophotometer. The scheme of the measurements is shown in Fig. 7.

[1] Peter Zijlstra, Pedro M. R. Paulo, and Michel Orrit, Optical detection of single non-absorbing molecules using the surface plasmon resonance of a gold nanorod, Nat. Nanotechnol. **7**, 379 (2012).

[2] Kathryn M. Mayer and Jason H. Hafner, Localized surface plasmon resonance sensors, Chem. Rev. **111**, 3828 (2011).

[3] G. A. Wurtz, Robert Pollard, and Anatoly V. Zayats, Optical Bistability in Nonlinear Surface-Plasmon Polaritonic Crystals, Phys. Rev. Lett. **97**, 057402 (2006).

[4] Alexander S. Shorokhov, Kirill I. Okhlopkov, Jörg Reinhold, Christian Helgert, Maxim R. Shcherbakov, Thomas Pertsch, and Andrey A. Fedyanin, Ultrafast control of third-order optical nonlinearities in fishnet metamaterials, Sci. Rep. **6**, 28440 (2016).

[5] Vladimir M. Shalaev and Satoshi Kawata, *Nanophotonics with Surface Plasmons* (Elsevier, New York, 2006).

[6] Sang Eon Han and Gang Chen, Optical absorption enhancement in silicon nanohole arrays for solar photovoltaics, Nano Lett. **10**, 1012 (2010).

[7] Hairen Tan, Rudi Santbergen, Arno H. M. Smets, and Miro Zeman, Plasmonic light trapping in thin-film silicon solar cells with improved self-assembled silver nanoparticles, Nano Lett. **12**, 4070 (2012).

[8] Menaka De Zoysa, Kenji Ishizaki, Yoshinori Tanaka, Hitoshi Sai, Koji Matsubara, and Susumu Noda, Enhanced efficiency of ultrathin (~500 nm)-film microcrystalline silicon photonic crystal solar cells, Appl. Phys. Express **10**, 012302 (2017).

[9] Naresh K. Emani, Ting-Fung Chung, Alexander V. Kildishev, Vladimir M. Shalaev, Yong P. Chen, and Alexandra Boltasseva, Electrical modulation of Fano resonance in plasmonic nanostructures using graphene, Nano Lett. **14**, 78 (2014).

[10] Jessica R. Piper and Shanhui Fan, Total absorption in a graphene monolayer in the optical regime by critical coupling with a photonic crystal guided resonance, ACS Photonics **1**, 347 (2014).

[11] S. Thongrattanasiri, F. H. L. Koppens, and F. J. G. De Abajo, Complete Optical Absorption in Periodically Patterned Graphene, Phys. Rev. Lett. **108**, 047401 (2012).

[12] Hugen Yan, Tony Low, Wenjuan Zhu, Yanqing Wu, Marcus Freitag, Xuesong Li, Francisco Guinea, Phaedon Avouris, and Fengnian Xia, Damping pathways of mid-infrared plasmons in graphene nanostructures, Nat. Photonics **7**, 394 (2013).

[13] Yuancheng Fan, Zhe Liu, Fuli Zhang, Qian Zhao, Zeyong Wei, Quanhong Fu, Junjie Li, Changzhi Gu, and Hongqiang Li, Tunable mid-infrared coherent perfect absorption in a graphene meta-surface, Sci. Rep. **5**, 13956 (2015).

[14] José Dintinger, Stéphane Klein, and Thomas W. Ebbesen, Molecule-surface plasmon interactions in hole arrays: Enhanced absorption, refractive index changes, and all-optical switching, Adv. Mater. **18**, 1267 (2006).

[15] Koray Aydin, Vivian E. Ferry, Ryan M. Briggs, and Harry A. Atwater, Broadband polarization-independent resonant light absorption using ultrathin plasmonic super absorbers, Nat. Commun. **2**, 517 (2011).

[16] M. U. Pralle, N. Moelders, M. P. McNeal, I. Puscasu, A. C. Greenwald, J. T. Daly, E. A. Johnson, T. George, D. S. Choi, I. El-Kady, and R. Biswas, Photonic crystal enhanced narrow-band infrared emitters, Appl. Phys. Lett. **81**, 4685 (2002).

[17] Thomas Søndergaard, Sergey I. Bozhevolnyi, Sergey M. Novikov, Jonas Beermann, Eloïse Devaux, and Thomas W. Ebbesen, Extraordinary optical transmission enhanced by nanofocusing, Nano Lett. **10**, 3123 (2010).

[18] P. Nyga, V. P. Drachev, Mark D. Thoreson, and Vladimir M. Shalaev, Mid-IR plasmonics and photomodification with Ag films, Appl. Phys. B **93**, 59 (2008).

[19] Mildred S. Dresselhaus, Gene Dresselhaus, P. C. Eklund, and A. M. Rao, *Carbon Nanotubes* (Springer, Dordrecht, 2000).

[20] Savas Berber, Young-Kyun Kwon, and David Tománek, Unusually High Thermal Conductivity of Carbon Nanotubes, Phys. Rev. Lett. **84**, 4613 (2000).

[21] Edward A. Laird, Fei Pei, Wei Tang, Gary A. Steele, and Leo P. Kouwenhoven, A high quality factor carbon nanotube mechanical resonator at 39 GHz, Nano Lett. **12**, 193 (2012).

[22] Jonathan N. Coleman, Umar Khan, Werner J. Blau, and Yurii K. Gun'ko, Small but strong: A review of the mechanical properties of carbon nanotube-polymer composites, Carbon **44**, 1624 (2006).

[23] Marcus Rinkiö, Andreas Johansson, Marina Y. Zavodchikova, J. Jussi Toppari, Albert G. Nasibulin, Esko I. Kauppinen, and Päivi Törmä, High-yield of memory elements from carbon nanotube field-effect transistors with atomic layer deposited gate dielectric, New J. Phys. **10**, 103019 (2008).

[24] Max M. Shulaker, Gage Hills, Nishant Patil, Hai Wei, Hong-Yu Chen, H.-S. Philip Wong, and Subhasish Mitra, Carbon nanotube computer, Nature (London) **501**, 526 (2013).

[25] Michael L. Geier, Julian J. McMorrow, Weichao Xu, Jian Zhu, Chris H. Kim, Tobin J. Marks, and Mark C. Hersam, Solution-processed carbon nanotube thin-film complementary static random access memory, Nat. Nanotechnol. **10**, 944 (2015).

[26] Fumiaki N. Ishikawa, Hsiao-Kang Chang, Koungmin Ryu, Po-Chiang Chen, Alexander Badmaev, Lewis Gomez De Arco, Guozhen Shen, and Chongwu Zhou, Transparent electronics based on transfer printed aligned carbon nanotubes on rigid and flexible substrates, ACS Nano **3**, 73 (2009).

[27] Dong-Ming Sun, Marina Y. Timmermans, Ying Tian, Albert G. Nasibulin, Esko I. Kauppinen, Shigeru Kishimoto, Takashi Mizutani, and Yutaka Ohno, Flexible high-performance carbon nanotube integrated circuits, Nat. Nanotechnol. **6**, 156 (2011).

[28] K. F. Akhmadishina, I. I. Bobrinetskii, R. A. Ibragimov, I. A. Komarov, A. M. Malovichko, V. K. Nevolin, and V. A. Petukhov, Fabrication of flexible transparent conductive coatings based on single-walled carbon nanotubes, Inorg. Mater. (USSR) **50**, 23 (2014).

[29] Xuan Cao, Yu Cao, and Chongwu Zhou, Imperceptible and ultraflexible p-type transistors and macroelectronics based on carbon nanotubes, ACS Nano **10**, 199 (2016).

[30] Jianfeng Li, Liangbing Hu, Lian Wang, Yangxin Zhou, George Grüner, and Tobin J. Marks, Organic light-emitting diodes having carbon nanotube anodes, Nano Lett. **6**, 2472 (2006).

[31] Shuang Liang, Ze Ma, Gongtao Wu, Nan Wei, Le Huang, Huixin Huang, Huaping Liu, Sheng Wang, and Lian-Mao Peng, Microcavity-integrated carbon nanotube photodetectors, ACS Nano **10**, 6963 (2016).

[32] Yang Liu, Sheng Wang, Huaping Liu, and Lian-Mao Peng, Carbon nanotube-based three-dimensional monolithic optoelectronic integrated system, Nat. Commun. **8**, 15649 (2017).

[33] Irati Soto Lamata, Pablo Alonso-González, Rainer Hillenbrand, and Alexey Yu. Nikitin, Plasmons in cylindrical 2D materials as a platform for nanophotonic circuits, ACS Photonics **2**, 280 (2015).

[34] Zhiwen Shi, Xiaoping Hong, Hans A. Bechtel, Bo Zeng, Michael C. Martin, Kenji Watanabe, Takashi Taniguchi, Yuen-Ron Shen, and Feng Wang, Observation of a

Luttinger-liquid plasmon in metallic single-walled carbon nanotubes, Nat. Photonics **9**, 515 (2015).

[35] L. Martín-Moreno, F. J. García de Abajo, and F. J. García-Vidal, Ultraefficient Coupling of a Quantum Emitter to the Tunable Guided Plasmons of a Carbon Nanotube, Phys. Rev. Lett. **115**, 173601 (2015).

[36] Takahiro Morimoto, Soon-Kil Joung, Takeshi Saito, Don N. Futaba, Kenji Hata, and Toshiya Okazaki, Length-dependent plasmon resonance in single-walled carbon nanotubes, ACS Nano **8**, 9897 (2014).

[37] J. T. Hong, D. J. Park, J. H. Yim, J. K. Park, Ji-Yong Park, Soonil Lee, and Y. H. Ahn, Dielectric constant engineering of single-walled carbon nanotube films for metamaterials and plasmonic devices, J. Phys. Chem. Lett. **4**, 3950 (2013).

[38] Xiaowei He, Naoki Fujimura, J. Meagan Lloyd, Kristopher J. Erickson, A. Alec Talin, Qi Zhang, Weilu Gao, Qijia Jiang, Yukio Kawano, Robert H. Hauge, François Léonard, and Junichiro Kono, Carbon nanotube terahertz detector, Nano Lett. **14**, 3953 (2014).

[39] Mikhail E. Itkis, Ferenc Borondics, Aiping Yu, and Robert C. Haddon, Bolometric infrared photoresponse of suspended single-walled carbon nanotube films, Science **312**, 413 (2006).

[40] Gustavo Vera-Reveles, Trevor J. Simmons, Mariela Bravo-Sánchez, M. A. Vidal, Hugo Navarro-Contreras, and Francisco J. González, High-sensitivity bolometers from self-oriented single-walled carbon nanotube composites, ACS Appl. Mater. Interfaces **3**, 3200 (2011).

[41] Alexander Y. Glamazda, Victor Karachevtsev, William B. Euler, and Igor A. Levitsky, Achieving high mid-IR bolometric responsivity for anisotropic composite materials from carbon nanotubes and polymers, Adv. Funct. Mater. **22**, 2177 (2012).

[42] Trevor J. Simmons, Gustavo Vera-Reveles, Gabriel González, José Manuel Gutiérrez-Hernández, Robert J. Linhardt, Hugo Navarro-Contreras, and Francisco J. González, Bolometric properties of semiconducting and metallic single-walled carbon nanotube composite films, ACS Photonics **2**, 334 (2015).

[43] Gustavo E. Fernandes, Jin Ho Kim, Ashok K. Sood, and Jimmy Xu, Giant temperature coefficient of resistance in carbon nanotube/phase-change polymer nanocomposites, Adv. Funct. Mater. **23**, 4678 (2013).

[44] Kan Fu, Richard Zannoni, Chak Chan, S. H. Adams, John Nicholson, Eric Polizzi, and K. S. Yngvesson, Terahertz detection in single wall carbon nanotubes, Appl. Phys. Lett. **92**, 033105 (2008).

[45] M. Mahjouri-Samani, Y. S. Zhou, X. N. He, W. Xiong, P. Hilger, and Y. F. Lu, Plasmonic-enhanced carbon nanotube infrared bolometers, Nanotechnology **24**, 035502 (2013).

[46] Anna Moisala, Albert G. Nasibulin, David P. Brown, Hua Jiang, Leonid Khriachtchev, and Esko I. Kauppinen, Single-walled carbon nanotube synthesis using ferrocene and iron pentacarbonyl in a laminar flow reactor, Chem. Eng. Sci. **61**, 4393 (2006).

[47] Elena S. Zhukova, Artem K. Grebenko, Anton V. Bubis, Anatolii S. Prokhorov, Mikhail A. Belyanchikov, Alexey P. Tsapenko, Evgenia Gilshteyn, Daria S. Kopylova, Yury G. Gladush, Anton S. Anisimov, Vladimir B. Anzin, Albert G. Nasibulin, and Boris P. Gorshunov, Terahertz-infrared electrodynamics of single-wall carbon nanotube films, Nanotechnology **28**, 445204 (2017).

[48] Antonio Rogalski, *Infrared Detectors* (CRC Press, Boca Raton, FL, 2010).

[49] D. S. Kopylova, N. Yu. Boldyrev, V. Ya. Iakovlev, Yu. G. Gladush, and Albert G. Nasibulin, A bolometer based on single-walled carbon nanotubes and hybrid materials, Quantum Electron. **46**, 1163 (2016).

[50] Sergei G. Tikhodeev, A. L. Yablonskii, E. A. Muljarov, Nikolay A. Gippius, and Teruya Ishihara, Quasiguided modes and optical properties of photonic crystal slabs, Phys. Rev. B **66**, 045102 (2002).

[51] R. H. Ritchie, Plasma losses by fast electrons in thin films, Phys. Rev. **106**, 874 (1957).

[52] Junbo Gong, Rucheng Dai, Zhongping Wang, and Zengming Zhang, Thickness dispersion of surface plasmon of Ag nano-thin films: Determination by ellipsometry iterated with transmittance method, Sci. Rep. **5**, 9279 (2015).

[53] A. K. Petrov, V. O. Bessonov, K. A. Abrashitova, N. G. Kokareva, K. R. Safronov, A. A. Barannikov, P. A. Ershov, N. B. Klimova, I. I. Lyatun, V. A. Yunkin, M. Polikarpov, I. Snigireva, A. A. Fedyanin, and A. Snigirev, Polymer x-ray refractive nano-lenses fabricated by additive technology, Opt. Express **25**, 14173 (2017).